Journal of Vacuum Science and Technology A

RESEARCH ARTICLE | MARCH 07 2024

Interlayer registry effects on the electronic and piezoelectric properties of transition metal dichalcogenide bilayers

Special Collection: Celebrating the Achievements and Life of Joe Greene

S. R. J. Likith ✉; Geoff L. Brennecka ; Cristian V. Ciobanu

J. Vac. Sci. Technol. A 42, 032201 (2024)
https://doi.org/10.1116/6.0003264

JVST A
Journal of Vacuum Science & Technology A

ARTICLE

pubs.aip.org/avs/jva

Interlayer registry effects on the electronic and piezoelectric properties of transition metal dichalcogenide bilayers

Cite as: J. Vac. Sci. Technol. A 42, 032201 (2024); doi: 10.1116/6.0003264
Submitted: 30 October 2023 · Accepted: 8 February 2024 ·
Published Online: 7 March 2024

S. R. J. Likith,[1,a)] Geoff L. Brennecka,[2] and Cristian V. Ciobanu[1]

AFFILIATIONS

[1]Department of Mechanical Engineering, Colorado School of Mines, Golden, Colorado 80401
[2]Department of Metallurgical and Materials Engineering, Colorado School of Mines, Golden, Colorado 80401

Note: This paper is part of the Special Topic Collection Celebrating the Achievements and Life of Joe Greene.
[a)]**Authors to whom correspondence should be addressed:** jailikith@gmail.com; gbrennec@mines.edu; and cciobanu@mines.edu

ABSTRACT

Transition metal dichalcogenides (TMDC) are currently drawing significant interest from the scientific community as 2D materials that have intrinsically semiconducting bandgaps. One additional advantage of TMDCs for discovering and developing materials with novel electronic, electromechanical, or optoelectronic properties is that both layer composition and registry can be readily tailored. To understand how such tailoring can expand the range of properties, here we used density functional theory calculations to determine the electronic structure and piezoelectric properties of bilayer TMDC heterostructures based on MoX_2 and WX_2, where X can be S, Se, or Te. For identical layers with no misorientation with respect to one another, we find that the registry of the two layers can change the bandgap type (direct vs indirect), as well as its value (by ≈0.25 eV). We report similar conclusions for bilayer heterostructures in which the composition of the two layers is different. Interlayer registry also has a pronounced effect on piezoelectric properties as the piezoelectric coefficients of the two layers either nearly cancel each other or add up to yield enhanced values for the associated TMDC bilayer heterostructures. These results may serve as a guide for enhancing electronic and piezoelectric properties by stacking TMDC layers.

I. INTRODUCTION

Transition metal dichalcogenides (TMDCs) have a wide range of properties that are of fundamental and technological interest;[1–4] in particular, they entered the scene of 2D materials as the semiconductor counterpart of graphene (semimetal) and hexagonal boron nitride (insulator). Their properties include electronic band structure tunability and high-mobility charge carriers,[5–10] excitonic effects,[11] etc.—making TMDCs a very promising material for future optoelectronic devices. The electronic[12] and piezoelectric[13] properties of TMDCs have also made them attractive candidates for digital electronic devices,[14] flexible electrodes,[15] and sensors,[16] to name a few. In their monolayer form, TMDCs have been reported to have direct bandgaps.[17,18] In addition, TMDC monolayers have also been discovered to show piezoelectric responses that are comparable in magnitude to other 2D materials like h-BN, as well as to well-known 3D piezoelectric materials, including bulk wurtzite AlN and α-quartz.[19] Since the current applications market is currently covered by only a handful of technologically relevant piezoelectrics, there is a significant interest in expanding the set of useful piezoelectrics so as to unlock a wider range of properties and novel applications. As such, discovering new 2D materials[20] and stacking known TMDC materials to form heterostructures[21] are viable avenues for attaining enhanced piezoelectric responses. A key enabling factor for the increasing popularity of TMDCs, as well as their heterostructures, was the development of experimental techniques such as Chemical Vapor Deposition (CVD)[22] and atomic layer deposition[23] that have enabled the fabrication of monolayer and bilayer TMDCs.

Bulk TMDC semiconductors (e.g., MoS_2 and WS_2) are semiconducting, van der Waals layered materials;[24–27] despite being semiconductors, they are not piezoelectrics because their bulk structure is centrosymmetric. However, in the monolayer or few-layer form, TMDCs are not centrosymmetric anymore and display

a piezoelectric response. Apart from thickness control (which, incidentally, also affects their bandgap) other symmetry breaking factors that can enable piezoelectricity are compositional variations from a layer to another,[28] compositional disorder within layers,[29] different chalcogens on the different faces of the same monolayer (Janus layers);[30] in addition, it is conceivable that registry variations may also affect piezoelectricity, whether such variations occur via interlayer translations or interlayer twists.[31] A particular appeal of TMDC heterostructures from the ability to stack or grow individual TMDC monolayers on top of one another, and, in doing so, tailoring the properties of the resulting heterostructure to potentially meet specific needs. For instance, Liu *et al.* explored the assembly of van der Waals heterostructures and their use in various electronic devices such as light-harvesting and detection devices and highly flexible electrodes.[32] While there have been first-principles studies focused on the electronic[33–36] as well as piezoelectric properties,[28] a systematic study of TMDC heterostructure properties is desirable so we can have a better insight into the properties that are expected from heterostructures assembled from various TMDC monolayers.

In this article, we use density functional theory (DFT) calculations to explore the electronic and piezoelectric properties of heterostructures that consists of two TMDC monolayers, each with the composition MX_2 (where M: Mo, W and X: S, Se, Te). Using these monolayers as building blocks, we study the effects of composition on the electronic as well as the piezoelectric properties of these van der Waals heterostructures. In addition, since it has been established that the relative stacking registries of the layers play an important role in deciding the properties of the resulting heterostructures,[30] we also change the stacking of the constituent layers in each heterostructure to study its effects on the resulting electronic and piezoelectric properties. We expect that the heterostructures that are assembled from closely lattice matched monolayers to be of greater relevance for future experimental studies since the constituent layers are not unduly influenced by computational artifacts, i.e., by the strain associated with periodic boundary conditions in the DFT calculations. In doing so, we find that since the Γ and K points on the electronic band structures of these low strain heterostructures are very close to the Fermi energy, it is possible to change their bandgaps from direct to indirect (and vice versa) by changing the stacking sequence. In addition, we also find that certain stacking sequences allow the individual polarizations of the constituting monolayers of a heterostructure to add up, thus enhancing the piezoelectric coefficients of the heterostructures compared to the TMDC monolayers.

II. LAYER STRUCTURES AND COMPUTATIONAL DETAILS

For ease of describing the stacking of TMDC layers, we borrow nomenclature from the face-centered cubic (fcc) crystal structure and identify three atomically planar, triangular lattices.[37] The atoms of each such planar lattice in a TMDC monolayers are located above or below the hollow sites of the other two lattices [Fig. 1(a)]. These triangular lattices are labeled here a, b, and c (A, B, and C) when occupied by chalcogen (metal) atoms. We start by labeling the lower metal lattice by A, and then apply this labeling convention within that monolayer layer (e.g., one TMDC layer has a bAb stacking), as well as across the vdW gap between the TMDC layers. Thus, any bulk or bilayer structure consisting of two MX_2 layers (total of six atomic layers/planes) in the unit cell is denoted by a sequence of six letters. For example, the 2H TMDC bulk phase has the stacking bAb–aBa (lower layer-upper layer). In a TMDC bilayer, the placement of the second layer on top of the first can be achieved in six different high-symmetry stacking sequences, which are shown in Figs. 1(b)–1(g). We perform full lattice and atomic relaxations for the bilayer structures in all stacking sequences (Fig. 1) and all possible compositions of the individual layers, which yields 216 structures [6 stackings × 6 compositions (first layer) × 6 compositions (second layer)]. It is worth noting that the present study considers offset stacking only, but the same approach could be extended in the future to look at the effects of twist angles of similar heterostructures.

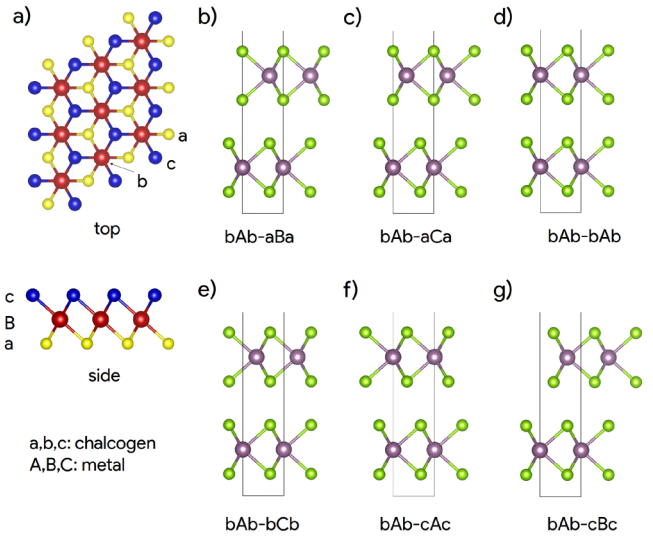

FIG. 1. (a) Top and side views of planar a, b, and c triangular lattices that can make up an MX_2 layer; capital (lower case) letters are used when a lattice is occupied by metal (chalcogen) atoms. (b)–(g). Side views of the six high-symmetry stacking sequences describing bilayer TMDC heterostructures.

We have performed first-principles calculations on TMDC bulk and bilayer heterostructures using DFT within the framework of the generalized gradient approximation (GGA) with projector-augmented wave (PAW) pseudopotentials,[38] as implemented in the Vienna *Ab initio* Simulation Package (VASP).[39] In order to capture the vdW interactions between layers, we have used the optB86b functional[40,41] when performing structural relaxations, band structure, and piezoelectric coefficient calculations. We have sampled the first Brillouin zone using a Γ-centered 16 × 16 × 1 (16 × 16 × 5) grid for the bilayer (bulk) structures calculations. We have used a plane wave energy cutoff of 540 eV, an energy criterion of 10^{-8} eV for electronic convergence and a force criterion of 10^{-3} eV/Å for ionic convergence. For the bilayer structures, we introduce a vacuum spacing of 18 Å along the *c*-axis in the supercell.

In the bulk 2H phase, the TMDCs have lattice constants that are largely dictated by the chalcogen species. Our 2H phase lattice

TABLE I. Lattice constants of the 2H bulk phase (bAb–aBa) of MX_2 crystals.

	a (Å)	c (Å)
MoS_2	3.167 (3.18,[a] 3.160[b])	12.370 (13.84[a], 12.294[b])
$MoSe_2$	3.300 (3.318,[a] 3.299[b])	13.047 (14.63[a], 12.938[b])
$MoTe_2$	3.528 (3.552,[a] 3.522[b])	14.063 (14.955[a], 13.968[b])
WS_2	3.167 (3.182,[a] 3.153[c])	12.433 (13.873[a], 12.323[c])
WSe_2	3.299 (3.317,[a] 3.282[c])	13.115 (14.926[a], 12.96[c])
WTe_2	3.530 (3.550,[a] 3.600[d])	14.113 (14.919[a], 14.18[d])

[a]Reference 42.
[b]Reference 43.
[c]Reference 44.
[d]Reference 45.

constants computed using optB86b functional[40,41] are consistent to the existing literature (Table I). When creating bilayer heterostructures for the DFT calculations, we necessarily introduce strain in each layer due to periodic boundary conditions that require the use of one common lattice constant a, regardless of the fact that the individual TMDC layers may have a different parameter, e.g., a_1 and a_2. We define the strain in a heterostructure ε_h as the average of the absolute values of the strains in each layer, $\varepsilon_h = (1/2)(|a - a_1|/a_1 + |a - a_2|/a_2)$. It should be specified that we are not searching for global structural minima of the 2D structures[46,47] but use the layer nomenclature described above to exhaustively explore all the non-equivalent registries that can be created with two TMDC monolayers. When creating the TMDC bilayers, we identify three categories: low strain (created from TMDC layers having the same chalcogen, but for which the metal can be the same or different), intermediate strain (from one layer with chalcogens S and the other with Se), and high strain (chalcogen pairs Se, Te or S, Te) heterostructures. These combinations and the associated value of strain are depicted in Fig. 2, where there are four levels of strains expected with, e.g., a strain of 2% indicating that we a priori expect one layer to be biaxially stretched by 2% and the other biaxially compressed by the same amount. The results corresponding to low and intermediate heterostructure strain ε_h are more likely to be representative of the actual structure and properties of TMDC bilayers in experimental situations.

III. RESULTS

A. Relative stability of bilayer heterostructures

First, we assess the relative stability of the different stackings in the absence of heterostructure strain, i.e., for the case in which both layers have the same composition. We compute the energies of the six registries identified in Figs. 1(b)–1(g), relative to the bAb–aBa bilayers. These relative energies are listed in Table II.

As shown in Table II, the most stable stackings are those in which the metal layers are on two different sublattices and the chalcogen sublattices across the vdW gap are also different (bAb–aBa, bAb–aCa, and bAb–cBc). If the metal atoms occupy the same sublattice in the two bilayers, and/or the chalcogen atoms are exactly in registry with each other across the vdW gap, the energy of the bilayers are significantly higher (Table II). These results indicate

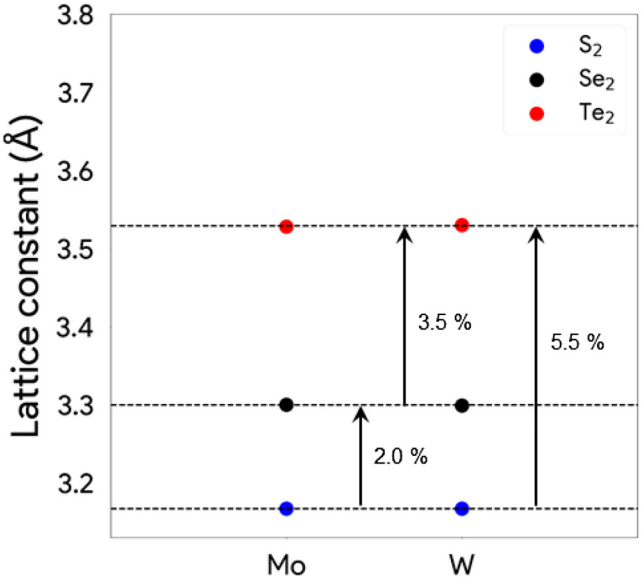

FIG. 2. Expected values of layer strain ε_h in bilayer heterostructure TMDCs where the metal can be Mo or W and the chalcogens S, Se, or Te. In DFT calculations, the use of periodic boundary conditions requires a common lattice constant hence a strain in each layer of a bilayer heterostructure.

that the vdW bonding mimics, perhaps fortuitously, the tendency of metallic bonds in fcc systems to maximize the number of first-order neighbors, only here some of the "neighbors" are seen across the vdW gap. Different chalcogen sublattices across the gap means that chalcogens in one layer are exactly above the hollow sites in the other layer, strengthening the binding between the two layers: in other words, there is some directionality to the vdW interactions and they cannot be reduced to a simple function of the interlayer spacing. Another trend emerging from Table II is that the effect of interlayer registry (layer stacking) is more pronounced as we go from sulfides, to selenides, to tellurides. This is an indication that the size of the chalcogen shapes the landscape of the vdW energy between the TMDC layers. As apparent from Table II, the effect of chalcogen size and that of changing the stacking between layer are comparable to each other in terms of determining the relative stability of the bilayers.

TABLE II. Calculated energies ΔE (meV per unit formula), relative to the most stable configuration, for bilayer MX_2 in the six stacking sequences shown in Fig. 1.

Stacking	MoS_2	$MoSe_2$	$MoTe_2$	WS_2	WSe_2	WTe_2
bAb–aBa	0.00	0.00	0.00	0.00	0.00	0.00
bAb–aCa	0.39	1.65	6.65	1.37	2.89	8.25
bAb–cBc	0.40	1.64	6.66	1.37	2.88	8.26
bAb–cAc	8.37	14.69	39.44	9.96	17.04	43.76
bAb–bCb	34.14	37.76	50.54	33.34	37.10	50.48
bAb–bAb	58.78	76.35	129.25	57.99	74.90	127.98

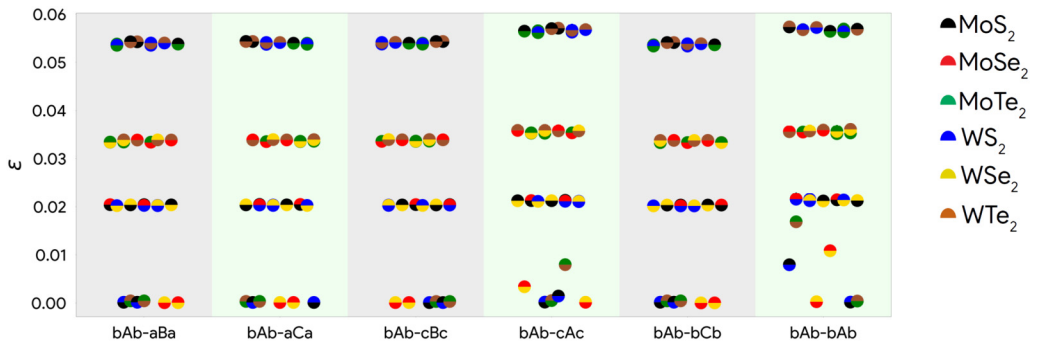

FIG. 3. Computed average strains in the layers of all heterostructures studied in the present work.

TABLE III. Electronic bandgaps of the 2H bulk phase (bAb–aBa) of MX_2 crystals.

	Present work (eV)	Other Works (eV)
MoS_2	0.89	0.7[a],0.75[b],1.23[c]
$MoSe_2$	0.85	0.75[a],0.8[b],1.09[c]
$MoTe_2$	0.72	0.66[b],1.0[d]
WS_2	1.01	0.89[b],1.35[d]
WSe_2	0.97	0.97[b],1.20[d]
WTe_2	0.79	0.81[b]

[a]Reference 48.
[b]Reference 49.
[c]Reference 50.
[d]Reference 51.

Another important effect that we have investigated is that of heterostructuring, i.e., different compositions of the two TMDC layers. The calculated strain ε_h after relaxation is displayed in Fig. 3. The DFT calculations for all stacking and compositions indeed bear out our expectation of four values of bilayer strain, with a few exceptions pertaining to metal lattices in registry to each other (bAb–cAc and bAb–bAb, refer to Fig. 3). As mentioned above, in this case, there are artifacts brought by the periodic boundary conditions (which impose large strains on each layer), so we will focus on the results pertaining to low and intermediate strain bilayers.

B. Electronic properties

Before analyzing the electronic properties of heterostructures, we first compute the electronic bandgap of the parent structures, i.e., the bulk phases of TMDC. These results are summarized in Table III and show a variation both in the value of the bandgap and in its character (direct or indirect). The bandgap variations are, however, not particularly large (from 0.79 to 1.01 eV). With an aim

TABLE IV. Magnitude (eV) and transition of the electronic bandgaps of the zero-strain structures in the present work.

	MoS_2	$MoSe_2$	$MoTe_2$	WS_2	WSe_2	WTe_2	MoS_2–WS_2	$MoSe_2$–WSe_2	$MoTe_2$–WTe_2
bAb–aBa	1.30	1.19	0.97	1.45	1.35	1.03	1.26	1.24	0.96
	Γ–Φ[a]	Γ–Φ	Γ–Ψ[b]	Γ–Φ	Γ–Φ	K–Ψ	Γ–K	Γ–Φ	K–Φ
bAb–aCa	1.27	1.20	1.02	1.47	1.38	1.07	1.20	1.23	0.92
	Γ–K	Γ–Φ	Γ–Ψ	Γ–Φ	Γ–Φ	K–K	Γ–K	Γ–Φ	K–K
bAb–cBc	1.27	1.20	1.02	1.46	1.38	1.07	1.26	1.28	1.03
	Γ–K	Γ–Φ	Γ–Ψ	Γ–Φ	Γ–Φ	K–K	Γ–K	Γ–Φ	K–K
bAb–cAc	1.32	1.27	0.97	1.52	1.45	0.96	1.25	1.25	1.04
	Γ–K	Γ–Ψ	K–K	Γ–Φ	Γ–Φ	K–K	Γ–K	K–K	K–K
bAb–bCb	1.56	1.42	1.095	1.70	1.48	1.14	1.45	1.31	0.97
	Γ–K	K–Φ	K–Ψ	Γ–Φ	K–Φ	K–K	Γ–K	K–Φ	K–K
bAb–bAb	1.46	1.31	0.86	1.65	1.39	0.84	1.38	1.14	0.97
	Γ–K	K–Φ	K–K	Γ–K	K–Φ	K–K	Γ–K	K–K	K–K

[a]$\Phi \equiv (0.175, 0.175, 0)$.
[b]$\Psi \equiv (0.193, 0.193, 0)$ in reciprocal space.

TABLE V. Magnitude (eV) and transition of the electronic bandgaps of the 2% strain structures in the present work.

	MoS_2–$MoSe_2$	WS_2–WSe_2	MoS_2–WSe_2	WS_2–$MoSe_2$
bAb–aBa	0.82	0.93	0.64	1.11
	K–K	K–K	K–K	K–K
bAb–aCa	0.76	0.87	0.58	1.06
	K–K	K–K	K–K	K–K
bAb–cBc	0.87	0.98	0.69	1.11
	Γ–K	K–K	K–K	Γ–K
bAb–cAc	0.80	0.90	0.61	0.11
	K–K	K–K	K–K	K–K
bAb–bCb	0.77	0.90	0.58	1.10
	K–K	K–K	K–K	K–K
bAb–bAb	0.75	0.87	0.54	1.11
	K–K	K–K	K–K	K–K

toward tuning the bandgap over a wider range of values, we have calculated the bandgaps of all bilayers structures with the six stacking sequences. The bandgap results for bilayers with low (∼0.0%) and intermediate (∼2%) strain are shown in Tables IV and V, respectively.

The computed electronic bandgaps of the bilayer TMDC heterostructures, as well as the parent bilayer structures, are shown in Figs. 4(a) and 4(b), for direct and indirect bandgaps, respectively. The range for direct (indirect) bandgaps extends to ≈1.3 (1.7 eV), but there is no discernable correlation between bandgap values and stacking in Fig. 4.

First, we note that among the parent bilayer structures, $MoTe_2$ shows a direct (K–K) bandgap in two low-stability stackings (bAb–cAc: 0.86 eV; bAb–bAb: 0.97 eV), and WTe_2 shows a direct (K–K) bandgap in all but one (bAb–aBa) stacking sequences. This indicates that having Te in the structure can lead to direct bandgaps in the parent bilayer structures. This is also seen in Te-containing (near)zero-strain heterostructures, as shown in Table IV. Tables IV and V show the magnitude as well as the transition of the bandgaps of the low strain (≤3%) heterostructures in the six different stacking sequences arranged in decreasing order of stability. Typical band structures are shown in Fig. 5, illustrating four types of transitions present in low-strain heterostructures.

$MoTe_2$–WTe_2 heterostructures have a direct (K–K) band gap in all but one (bAb–aBa) stacking sequence. Most of the low strain heterostructures shown in Tables IV and V have a direct (K–K) bandgap across most stacking sequences. Some exceptions to this include the MoS_2–WS_2 heterostructure that shows an indirect (Γ–K) bandgap across all the stacking sequences, and the MoS_2–

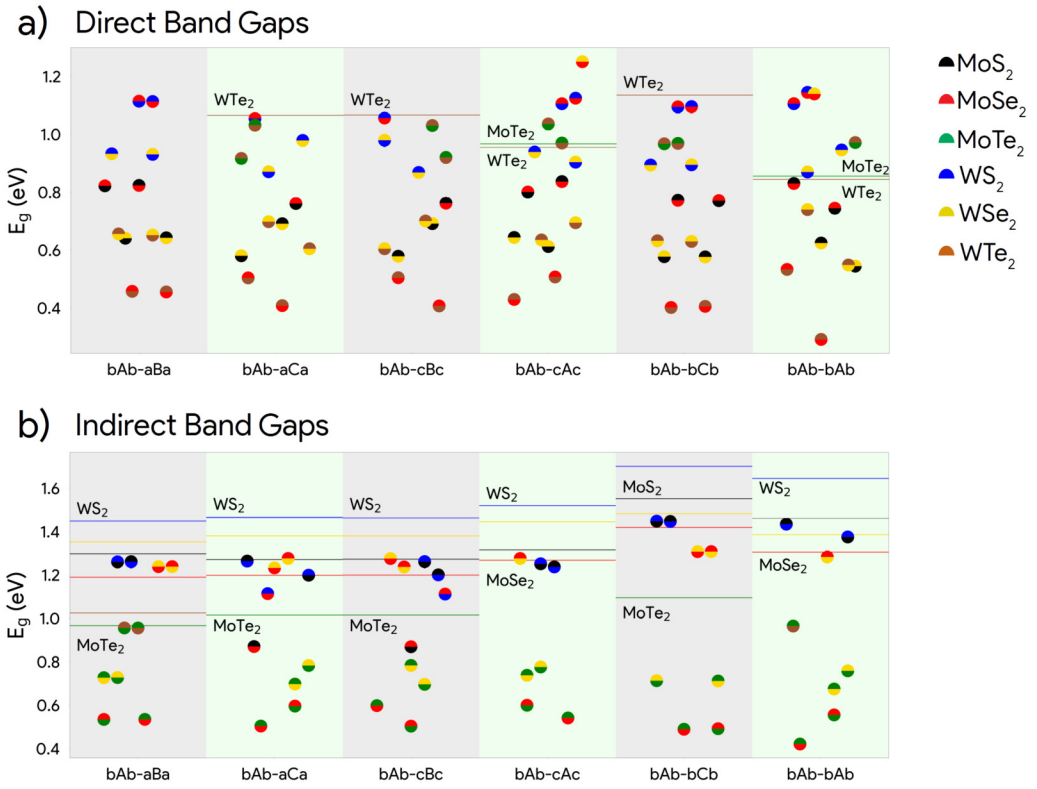

FIG. 4. Computed electronic bandgaps of heterostructures in six different stacking sequences. The bandgaps of the parent MX_2 bulk structures for a given stacking sequence are shown as solid lines. Structures with direct bandgaps are shown in (a) and those with indirect bandgaps are shown in (b).

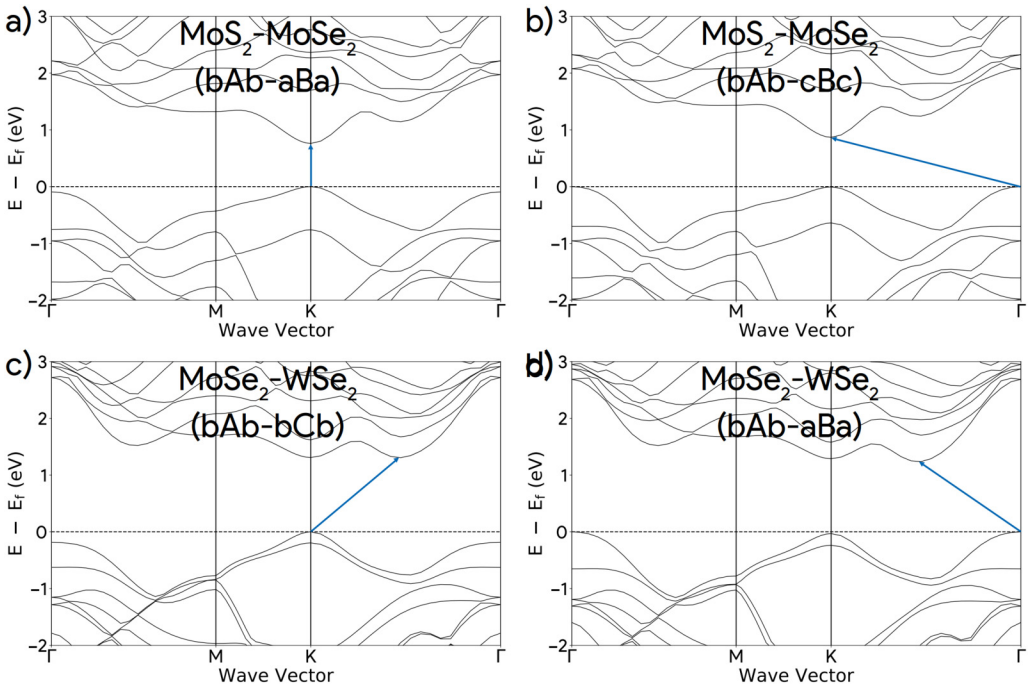

FIG. 5. Computed band structures showing four different types of transitions observed in low-strain heterostructures. The arrows correspond to the bandgaps, i.e., the lowest energy transitions between occupied and unoccupied states. (a) K–K (b), Γ–K, (c) K–Φ, (d) Γ–Φ.

$MoSe_2$ and WS_2–$MoSe_2$ heterostructures that show an indirect (Γ–K) band gap in only one stacking sequence, and a direct (K–K) band gap in all other stacking sequences. This behavior can be explained using the electronic band structures shown in Fig. 5. Figures 5(a) and 5(b) show the band structures of the MoS_2–$MoSe_2$ heterostructure in the bAb–aBa and bAb–cBc stacking sequences, respectively. While we see a direct (K–K) bandgap of 0.82 eV in the bAb–aBa stacking sequence, this can be easily tuned to an indirect (Γ–K) bandgap of 0.87 eV by stacking it in the bAb–cBc sequence, which is another high-stability stacking sequence. Next, we look at Figs. 5(c) and 5(d), which show the effect of changing the stacking sequence of the $MoSe_2$–WSe_2 heterostructure. While Fig. 5(c) shows the indirect (K–Φ) bandgap (1.31 eV) of the $MoSe_2$–WSe_2 heterostructure, this can be tuned to an indirect (Γ–Φ) bandgap of 1.24 eV by switching to the bAb–aBa stacking sequence. While we explore the band structure tuning in the MoS_2–$MoSe_2$ and the $MoSe_2$–WSe_2 heterostructures here, Tables IV and V shows that it is possible to tune the nature as well as the magnitude of the bandgap of a heterostructure by simply altering the stacking sequence. With this motivation, we list the stacking sequences in the decreasing order of stability for the low strain heterostructures studied here.

C. Piezoelectric properties

TMDCs typically occur in one of three polytypes: 1T, 2H, and 3R.[52] The tetragonal 1T polytype has a single layer unit cell that is stacked in the aBc sequence. This phase has been shown to be metallic,[53] and hence, has not been of interest for piezoelectric applications. The hexagonal 2H phase consists of two layer unit cells that are stacked in the bAb–aBa sequence. The rhombohedral 3R polytype is made up of three layer unit cells in the bAb–cBc-aCa stacking sequence. On account of their electronic bandgaps being in the semiconductor range and their thermodynamic stability, the 2H-TMDCs are currently the most prominently studied.[54] However, bulk MX_2 compounds in the bAb–aBa stacking sequence (the 2H phase) are not piezoelectric since they possess an inversion center. We thus explore two different ways to break the centrosymmetry in order to obtain a piezoelectric response. One way is to change how the two layers of the unit cell are stacked relative to each other; another way to achieve a piezoelectric response is by changing the composition of one of the layers, i.e., to create MX_2–NY_2 heterostructures.

To evaluate the piezoelectric coefficient tensors, we utilize the density functional perturbation theory (DFPT)[55–57] method as implemented in VASP. The piezoelectric coefficient tensor e_{ij} relates the polarization, P_i $(i = 1, 2, 3)$ to the strain ε_j (using the Voigt notation[58] where $j = 1, 2, 3$) as[59]

$$P_i = e_{ij}\varepsilon_j. \tag{1}$$

The bulk heterostructures as well as their bilayer counterparts possess $3m$ (or higher) point group symmetry. This reduces the

TABLE VI. Piezoelectric coefficient e_{21} of bAb MX_2 monolayers.

	Present work (10^{-10}C/m)	Other works (10^{-10}C/m)
MoS_2	3.68	3.64[a],3.56[b],2.9[c]
$MoSe_2$	3.79	3.92[a],3.84[b]
$MoTe_2$	4.70	5.43[a],4.98[b]
WS_2	2.36	2.47[a],2.46[b]
WSe_2	2.51	2.71[a],2.66[b]
WTe_2	3.21	3.40[a],3.52[b]

[a]Reference 19.
[b]Reference 30.
[c]Reference 60.

TABLE VII. Computed piezoelectric coefficients e_{21} ($\times 10^{-10}$ C/m) of the MX_2 monolayers and bAb–aCa bilayers stacking sequence.

MX_2	bAb	bAb–aCa
MoS_2	3.57	7.09
$MoSe_2$	3.79	7.50
$MoTe_2$	4.70	9.24
WS_2	2.36	4.71
WSe_2	2.51	4.96
WTe_2	3.21	6.29

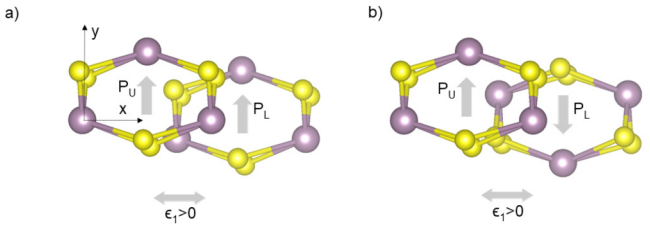

FIG. 6. Polarization values corresponding to the upper and lower layers upon straining along the *a* direction can either (a) add or (b)subtract when layers are stacked to form a homo- or heterostructure.

number of independent components of the piezoelectric coefficient tensor, e_{ij}. For the bulk structures (hexagonal unit cells), the piezoelectric coefficient tensor is

$$e_{ij} = \begin{pmatrix} 0 & 0 & 0 & 0 & e_{15} & e_{21} \\ e_{21} & -e_{21} & 0 & e_{15} & 0 & 0 \\ e_{31} & e_{31} & e_{33} & 0 & 0 & 0 \end{pmatrix}. \quad (2)$$

For the bilayer structures in 2D, Eq. (2) reduces to

$$e_{ij} = \begin{pmatrix} 0 & 0 & 0 & 0 & 0 & e_{21} \\ e_{21} & -e_{21} & 0 & 0 & 0 & 0 \\ e_{31} & e_{31} & 0 & 0 & 0 & 0 \end{pmatrix}. \quad (3)$$

We first calculate the piezoelectric coefficients for bAb monolayers (Table VI). Table VI also shows that are results are consistent with published computational and experimental literature studies.[19,30,60] The MX_2 monolayers act as building blocks for all the structures, as shown in Table VII. The piezoelectric coefficient $e_{21}^{(h)}$ of any structure built from two stacked monolayers MX_2 and NY_2 can be calculated using

$$e_{21}^{(h)} = e_{21}^{(1)} \pm e_{21}^{(2)}, \quad (4)$$

where e_{21}^{i} is the piezoelectric coefficient of the i monolayer. The sign on the second term is decided by the stacking sequence that is employed to build the structure (e.g., Fig. 6). Out of the six stacking sequences studied here, there are three stacking sequences (bAb–aCa, bAb–bAb, and bAb–cBc) wherein the polarization developed in the constituent monolayers are in the same direction, and hence, they add up to give a higher resultant polarization of the structure (compared to the monolayers). These are the stacking sequence where the piezoelectric coefficients of the constituent monolayers add up to give the piezoelectric coefficient of the structure. In the remaining three stacking sequences (bAb–aBa, bAb–bCb, and bAb–cAc), the polarization developed in the constituent monolayers are in opposite directions, and hence, they result in a smaller resultant polarization of the structure. For instance, we expect the piezoelectric coefficient of the MX_2 bilayers in any of the former

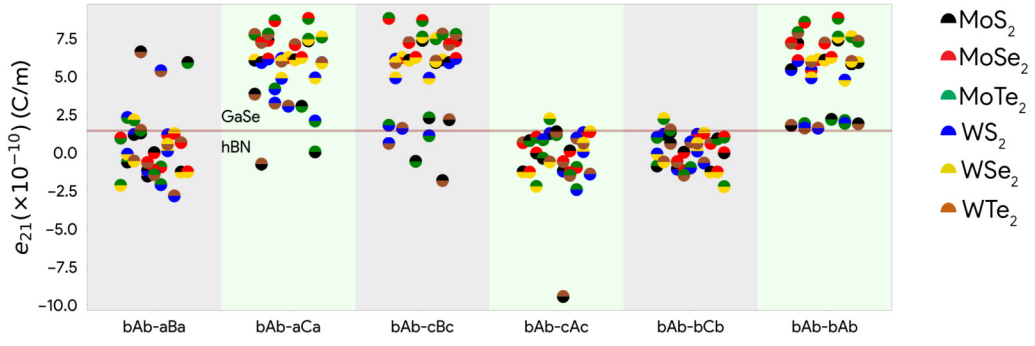

FIG. 7. Computed piezoelectric coefficients of the heterostructures in the six different stacking sequences studied in the present work. The piezoelectric coefficients of the parent MX_2 bilayer structures for a given stacking sequences are shown as solid lines. Structures with $e_{12} < 10^{-12}$ C/m are not shown.

three stacking sequences to be equal to twice the piezoelectric coefficient of the respective MX_2 monolayer. We compare the piezoelectric coefficients of the MX_2 monolayers and bilayers in one of these stacking sequences (bAb–aCa) in Table VII to verify this. Table VII shows that this expectation is born out, albeit in an approximate way—meaning that e_{21} for the bilayers in bAb–aCa, bAb–bAb, or bAb–cBc stackings is approximately double that of the monolayer. It is worth noting here that even though we present the piezoelectric coefficient values of the parent MX_2 bilayer structures, Eq. (4) holds for all the low strain ($\leq 3\%$) heterostructures studied here. At the same composition, within each group of stacking sequences, we see no variation in piezoelectric coefficients, thus indicating a weak coupling between layers across the van der Waals gap.

We have also computed e_{21} for all heterostructures and all stackings and summarized the results in Fig. 7, which show that e_{21} ranges approximately from -10 to $+10 \times 10^{-10}$ C/m. As an aside, we note that twisted 2D heterostructures[31] and 1D helical nanostructures[61,62] have non-colinear polarizations from one layer to the next. For such structures, the polarization cancelation shown in Fig. 6(b) is unlikely to occur, and we expect a spatially modulated piezoelectric response for such structures.

IV. CONCLUDING REMARKS

We note here that $MoTe_2$ has, in particular, gained special attention among TMDCs for various reasons. First, single and few layers $MoTe_2$ have been predicted to exhibit a larger carrier mobility compared to several other TMDCs at temperatures close to room temperature.[63] Furthermore, the piezoelectric response of $MoTe_2$, in its monolayer form, has been shown to be the highest of all the MX_2 monolayers included in the study by Duerloo *et al.*[19] In addition to these attractive properties, $MoTe_2$ has also been shown to be stable in the 2H phase at room temperature.[64] In this study, we show that heterostructuring of these TMDC monolayers, including $MoTe_2$, can further enhance the resultant piezoelectric response, in addition to offering an added level of control in modifying both the type (direct vs indirect) as well as the magnitude of their electronic bandgaps.

We have demonstrated how changing the composition and the stacking sequence of a TMDC hetersotructure allows us to go back and forth between direct and indirect electronic band gaps and also tune the magnitude of the bandgap. In addition, we show that strain is another important controlling parameter that can be used to alter the nature and magnitude of the bandgaps. This unlocks a fine level of control of the electronic properties of the TMDC heterostructures, thus helping their use in electronics applications. Furthermore, we show that stacking TMDC monolayers in certain ways allows for a larger piezoelectric response compared to that of the constituent layers. Thus, we use the effect of stacking sequences on TMDC heterostructures to harness higher piezoelectric responses in a class of materials that have already been known to show comparable piezoelectric responses to widely used, 3D piezoelectric materials such as α-quartz and bulk wurtzite AlN.[19] Similar studies can be carried out for the case of free-standing high-entropy sulfides,[65,66] monochalcogenides,[67] or substrate-supported 2D materials.[68] Therefore, we expect these results to serve as a stepping stone towards populating an extensive property database of TMDC heterostructures, and in doing so, enabling their widespread use in nanoscale applications.

ACKNOWLEDGMENTS

G.L.B. gratefully acknowledges the support of the National Science Foundation (NSF) through Grant No. DMR-2119281. All authors were supported for various parts of this work by NSF Grant. No. DMREF-1534503.

AUTHOR DECLARATIONS

Conflict of Interest

The authors have no conflicts to disclose.

Author Contributions

S. R. J. Likith: Data curation (lead); Formal analysis (equal); Investigation (lead). **Geoff L. Brennecka:** Formal analysis (equal); Funding acquisition (lead); Investigation (equal); Supervision (supporting). **Cristian V. Ciobanu:** Formal analysis (equal); Funding acquisition (supporting); Investigation (equal); Supervision (lead).

DATA AVAILABILITY

The data that support the findings of this study are available from the authors upon reasonable request.

REFERENCES

[1]K. S. Novoselov, D. Jiang, F. Schedin, T. J. Booth, V. V. Khotkevich, S. V. Morozov, and A. K. Geim, Proc. Natl. Acad. Sci. U.S.A. **102**, 10451 (2005).
[2]R. Mas-Ballesté, C. Gómez-Navarro, J. Gómez-Herrero, and F. Zamora, Nanoscale **3**, 20 (2011).
[3]M. Xu, T. Liang, M. Shi, and H. Chen, Chem. Rev. **113**, 3766 (2013).
[4]Se-Yang Kim, Jinsung Kwak, Cristian V. Ciobanu, and Soon-Yong Kwon, Adv. Mater. **31**, 1804939 (2019).
[5]A. Ebnonnasir, B. Narayanan, S. Kodambaka, and C. V. Ciobanu, Appl. Phys. Lett. **105**, 031603 (2014).
[6]A. Gupta, T. Sakthivel, and S. Seal, Prog. Mater. Sci. **73**, 44 (2015).
[7]S. Manzeli, D. Ovchinnikov, D. Pasquier, O. V. Yazyev, and A. Kis, Nat. Rev. Mater. **2**, 17033 (2017).
[8]A. Ayari, E. Cobas, O. Ogundadegbe, and M. S. Fuhrer, J. Appl. Phys. **101**, 014507 (2007).
[9]H.-P. Komsa, J. Kotakoski, S. Kurasch, O. Lehtinen, U. Kaiser, and A. V. Krasheninnikov, Phys. Rev. Lett. **109**, 035503 (2012).
[10]M. Chhowalla, Z. Liu, and H. Zhang, Chem. Soc. Rev. **44**, 2584 (2015).
[11]Ashwin Ramasubramaniam, Phys. Rev. B **86**, 115409 (2012).
[12]W. S. Yun, S. W. Han, S. C. Hong, I. G. Kim, and J. D. Lee, Phys. Rev. B **85**, 033305 (2012).
[13]M. M. Alyörük, Y. Aierken, D. Çakır, F. M. Peeters, and C. Sevik, J. Phys. Chem. C **119**, 23231 (2015).
[14]D. Jariwala, V. K. Sangwan, L. J. Lauhon, T. J. Marks, and M. C. Hersam, ACS Nano **8**, 1102 (2014).
[15]K. S. Kim, *et al.*, Nature **457**, 706 (2009).
[16]D. J. Late, *et al.*, ACS Nano **7**, 4879 (2013).
[17]F. Zahid, L. Liu, Y. Zhu, J. Wang, and H. Guo, AIP Adv. **3**, 052111 (2013).
[18]Q. H. Wang, K. Kalantar-Zadeh, A. Kis, J. N. Coleman, and M. S. Strano, Nat. Nanotechnol. **7**, 699 (2012).
[19]K.-A. N. Duerloo, M. T. Ong, and E. J. Reed, J. Phys. Chem. Lett. **3**, 2871 (2012).

[20]S. Manna, P. Gorai, G. L. Brennecka, C. V. Ciobanu, and V. Stevanović, "Large piezoelectric response of van der Waals layered solids," preprint arXiv:1804.10997 (2018).
[21]T. Niu and A. Li, Prog. Surf. Sci. **90**, 21 (2015).
[22]Y.-H. Lee, *et al.*, Adv. Mater. **24**, 2320 (2012).
[23]L. K. Tan, B. Liu, J. H. Teng, S. Guo, H. Y. Low, and K. P. Loh, Nanoscale **6**, 10584 (2014).
[24]A. K. Geim and I. V. Grigorieva, Nature **499**, 419 (2013).
[25]W. J. Yu, Z. Li, H. Zhou, Y. Chen, Y. Wang, Y. Huang, and X. Duan, Nat. Mater. **12**, 246 (2013).
[26]K. S. Novoselov, A. Mishchenko, A. Carvalho, and A. H. C. Neto, Science **353**, aac9439 (2016).
[27]S. J. Haigh, *et al.*, Nat. Mater. **11**, 764 (2012).
[28]S. Yu, Q. Rice, B. Tabibi, Q. Li, and F. J. Seo, Nanoscale **10**, 12472 (2018).
[29]Yulong Chen, *et al.*, Adv. Mater. **34**, 2201630 (2022).
[30]L. Dong, J. Lou, and V. B. Shenoy, ACS Nano **11**, 8242 (2017).
[31]Chendong Zhang, Chih-Piao Chuu, Xibiao Ren, Ming-Yang Li, Lain-Jong Li, Chuanhong Jin, Mei-Yin Chou, and Chih-Kang Shih, Sci. Adv. **3**, e1601459 (2017).
[32]Y. Liu, N. O. Weiss, X. Duan, H.-C. Cheng, Y. Huang, and X. Duan, Nat. Rev. Mater. **1**, 16042 (2016).
[33]B. Amin, N. Singh, and U. Schwingenschlögl, Phys. Rev. B **92**, 075439 (2015).
[34]L. Kou, T. Frauenheim, and C. Chen, J. Phys. Chem. Lett. **4**, 1730 (2013).
[35]M. Sharma, A. Kumar, P. K. Ahluwalia, and R. Pandey, J. Appl. Phys. **116**, 063711 (2014).
[36]K. Kośmider and J. Fernández-Rossier, Phys. Rev. B **87**, 075451 (2013).
[37]S. R. J. Likith, C. A. Farberow, S. Manna, A. Abdulslam, V. Stevanović, D. A. Ruddy, J. A. Schaidle, D. J. Robichaud, and C. V. Ciobanu, J. Phys. Chem. C **122**, 1223 (2018).
[38]G. Kresse and D. Joubert, Phys. Rev. B **59**, 1758 (1999).
[39]G. Kresse and J. Furthmüller, Phys. Rev. B **54**, 11169 (1996).
[40]J. Klimeš, D. R. Bowler, and A. Michaelides, J. Phys.: Condens. Matter **22**, 022201 (2009).
[41]J. Klimeš, D. R. Bowler, and A. Michaelides, Phys. Rev. B **83**, 195131 (2011).
[42]P. Johari and V. B. Shenoy, ACS Nano **5**, 5903 (2011).
[43]Th. Böker, R. Severin, A. Müller, C. Janowitz, R. Manzke, D. Voß, P. Krüger, A. Mazur, and J. Pollmann, Phys. Rev. B **64**, 235305 (2001).
[44]W. J. Schutte, J. L. De Boer, and F. Jellinek, J. Solid State Chem. **70**, 207 (1987).
[45]W. G. Dawson and D. W. Bullett, J. Phys. C: Solid State Phys. **20**, 6159 (1987).
[46]Cristian V. Ciobanu and Cristian Predescu, Phys. Rev. B **70**, 085321 (2004).
[47]C. V. Ciobanu, V. B. Shenoy, C. Z. Wang, and K. M. Ho, Surf. Sci. **544**, L715 (2003).
[48]A. H. Reshak and S. Auluck, Phys. Rev. B **71**, 155114 (2005).
[49]A. Kumar and P. K. Ahluwalia, Eur. Phys. J. B **85**, 186 (2012).
[50]K. K. Kam and B. A. Parkinson, J. Phys. Chem. **86**, 463 (1982).
[51]A. J. Grant, T. M. Griffiths, G. D. Pitt, and A. D. Yoffe, J. Phys. C: Solid State Phys. **8**, L17 (1975).
[52]A. V. Kolobov and J. Tominaga, "TMDC heterostructures," in *Two-Dimensional Transition-Metal Dichalcogenides* (Springer International Publishing Switzerland, 2016), pp. 447–471.
[53]F. Wypych and R. Schöllhorn, J. Chem. Soc., Chem. Commun. **19**, 1386 (1992).
[54]W. Zhao and F. Ding, Nanoscale **9**, 2301 (2017).
[55]S. Baroni, P. Giannozzi, and A. Testa, Phys. Rev. Lett. **58**, 1861 (1987).
[56]S. Baroni, S. De Gironcoli, A. Dal Corso, and P. Giannozzi, Rev. Mod. Phys. **73**, 515 (2001).
[57]X. Gonze, Phys. Rev. A **52**, 1096 (1995).
[58]W. Voigt, *Lehrbuch der Kristallphysik (mit Ausschluss der Kristalloptik)* (Springer, Leipzig, 2014).
[59]J. F. Nye, *Physical Properties of Crystals: Their Representation by Tensors and Matrices* (Oxford University, Oxford, 1985).
[60]H. Zhu, *et al.*, Nat. Nanotechnol. **10**, 151 (2015).
[61]Peter Sutter, Juan-Carlos Idrobo, and Eli Sutter, Adv. Funct. Mater. **31**, 2006412 (2021).
[62]Peter Sutter, Larousse Khosravi-Khorashad, Cristian V. Ciobanu, and Eli Sutter, Mater. Horiz. **10**, 3830 (2023).
[63]W. Zhang, Z. Huang, W. Zhang, and Y. Li, Nano Res. **7**, 1731 (2014).
[64]L. Zhou, *et al.*, J. Am. Chem. Soc. **137**, 11892 (2015).
[65]Aditya Deshpande, Christian Ratsch, Cristian V. Ciobanu, and Suneel Kodambaka, J. Appl. Phys. **131**, 234302 (2022).
[66]Koichi Tanaka, Hicham Zaid, Toshihiro Aoki, Aditya Deshpande, Koki Hojo, Cristian V. Ciobanu, and Suneel Kodambaka, Nano Lett. **24**, 493 (2024), PMID: 38148179.
[67]Sri Ranga Jai Likith and Cristian V. Ciobanu, Journal of Vacuum Science and Technology A **40**, 052202 (2022).
[68]H. S. Mok, A. Ebnonnasir, Y. Murata, S. Nie, K. F. McCarty, C. V. Ciobanu, and S. Kodambaka, Appl. Phys. Lett. **104**, 101606 (2014).